VENN DIAGRAM MULTI-LABEL CLASS INTERPRETATION OF DIABETIC FOOT ULCER WITH COLOR AND SHARPNESS ENHANCEMENT

A PREPRINT

Md Mahamudul Hasan
Department of Electrical and Electronic Engineering
Bangladesh University of Engineering and Technology
Dhaka 1205, Bangladesh
mahamudulrahat@gmail.com

Moi Hoon Yap
Department of Computing and Mathematics
Manchester Metropolitan University
Manchester M1 5GD, UK
m.yap@mmu.ac.uk

Md Kamrul Hasan*
Department of Electrical and Electronic Engineering
Bangladesh University of Engineering and Technology
Dhaka 1205, Bangladesh
khasan@eee.buet.ac.bd

ABSTRACT

Diabetic foot ulcer (DFU) is a severe complication of diabetes that can lead to amputation of the lower limb if not treated properly. Inspired by the 2021 Diabetic Foot Ulcer Grand Challenge (DFUC2021), researchers designed automated multi-class classification of DFU, including infection, ischaemia, both of these conditions, and none of these conditions. However, it remains a challenge as classification accuracy is still not satisfactory. This paper proposes a Venn Diagram interpretation of multi-label CNN-based method, utilizing different image enhancement strategies, to improve the multi-class DFU classification. We propose to reduce the four classes into two since both class wounds can be interpreted as the simultaneous occurrence of infection and ischaemia and none class wounds as the absence of infection and ischaemia. We introduce a novel Venn Diagram representation block in the classifier to interpret all four classes from these two classes. To make our model more resilient, we propose enhancing the perceptual quality of DFU images, particularly blurry or inconsistently lit DFU images, by performing color and sharpness enhancements on them. We also employ a fine-tuned optimization technique, adaptive sharpness-aware minimization (ASAM), to improve the CNN model's generalization performance. The proposed method is evaluated on the test dataset of DFUC2021, containing 5,734 images and the results are compared with the top-3 winning entries of DFUC2021. Our proposed approach outperforms these existing approaches and achieves Macro-Average F1, Recall and Precision scores of 0.6592, 0.6593, and 0.6652, respectively. Additionally, we achieve notable improvement in identifying infection and ischaemia. We perform ablation studies and image quality measurements to further interpret our proposed method. This proposed method will benefit patients with DFUs since it tackles the inconsistencies in captured images and can be employed for a more robust remote DFU wound classification and self-care of DFUs.

Keywords Diabetic foot ulcer · DFUC2021 · Deep learning · Medical images · Color and sharpness enhancement · Venn Diagram

*Corresponding author

1 Introduction

DFU is one of the most devastating complications associated with diabetes. According to International Diabetes Federation, about 537 million adults are living with diabetes and this number is expected to rise to 700 million adults by the year 2045 Sun et al. [2022]. Furthermore, patients with diabetes have a 15%-25% chance of developing DFUs, which affect between 9.1 million and 26.1 million people each year Armstrong et al. [2017]. If not managed properly, it can result in limb amputation and possibly death Ugwu et al. [2019]. To avoid serious health repercussions, patients with DFU must have regular checkups with their doctors, maintain personal hygiene, and take expensive medication. Patients and their families suffer immensely due to the devastating effects of DFUs on their emotional, physical, and financial well-being.

Currently, podiatrists and diabetes specialists undertake DFU assessments in foot clinics and hospitals which include: 1) maintaining track of the patient's medical history, 2) checking the wound extensively by an expert, 3) developing a treatment plan with the help of additional tests such as CT scans, MRIs, and X-rays. Furthermore, a wound is submitted for microbiological culture for signs of infection, and vascular assessment of the wound is carried out for ischaemia detection Cassidy et al. [2022]. These tests and resources are not available worldwide, especially in developing countries. Therefore, it puts a massive strain on developing countries' already overburdened healthcare infrastructure. A possible option would be to implement remote assessment of DFUs through foot images and encourage patients to self-care. However, Van Netten et al. van Netten et al. [2017] observed that doctors' validity and reliability were limited when assessing DFUs in remote foot images. Furthermore, the captured foot images are prone to blurring and inconsistent lighting, making it more challenging even for expert podiatrists to assess the DFUs correctly. To address these constraints, image enhancement techniques and computer vision approaches for classifying DFUs are necessary.

As computer vision and machine learning progress, their effect on medical imaging has increased significantly. Recently, it has been demonstrated that deep learning (DL) models perform better in detection, segmentation, and classification tasks on DFU images. Goyal et al. Goyal et al. [2020a] was the first to use CNN (DFUNet) for the classification of foot skin lesions between normal (healthy) and abnormal (DFU skin). However, the dataset contained only 1679 skin patches (1038 DFU and 641 healthy), and their proposed approach had difficulty classifying skin with a small DFU wound or having a red tone or wrinkles. In a later work Goyal et al. [2019], the author also showed the robustness of deep learning framework using faster region-based convolutional neural network (R-CNN) with InceptionV2 model for detection and localization of DFU patches. However, they used a small dataset of 1,775 DFU images, and their model also needed a post-processing stage to reduce false positives, making it unreliable for real-world use. In Goyal et al. [2020b], Goyal et al. introduced a dataset of 1459 images of patient's foot with DFU for binary classification of ischaemia and infection. They analyzed the performance of machine learning methods relative to deep learning methods. They demonstrated that deep learning methods outperformed traditional machine learning methods for binary classification of ischaemia and infection. However, their approach could not detect infection and ischaemia concurrently. Cassidy et al. Cassidy et al. [2021] presented a large DFU dataset of 4000 images. It was used in Diabetic Foot Ulcer Challenge 2020 (DFUC2020). A comprehensive evaluation of the deep learning methods in DFU detection is reported in Yap et al. [2021a]. In continuation of the challenge, Yap et al. Yap et al. [2021b] introduced a large multi-class DFU dataset which includes 15,683 DFU patches labeled with infection, ischaemia, both of these conditions, none of these conditions (control). The results of the DFUC2021 challenge are summarized by Cassidy et al. in Cassidy et al. [2022]. Galdran et al. Galdran et al. [2022], compared convolutional networks to Vision Transformers (ViT) and Data-efficient Image Transformers (DeiT). They employed Sharpness-Aware Minimization (SAM) Foret et al. [2020] for weight optimization, which resulted in a discernible improvement. However, a more effective optimization strategy known as Adaptive Sharpness-Aware Minimization (ASAM), recently introduced in Kwon et al. [2021], was unexplored. Bloch et al. Bloch et al. [2022] introduced a semi-supervised training strategy generating synthetic DFU images via pix2pixHD to overcome class imbalance. However, there was no metric or quality evaluation of the generated synthetic DFU images. Ahmed et al. Ahmed and Naveed [2022] proposed an ensemble of EfficientNet B0-B6, Resnet-50, and Resnet-101 architectures as backbone and designed a bias adjustable softmax activation layer to handle the class imbalance. However, adjusting bias at the inference level could not fully eliminate the bias introduced by weighted cross-entropy loss towards classes with high numbers of images. As a result, the ischaemia case with the lowest number of images performs the worst among all the other approaches.

This paper is aimed at solving the multi-class (i.e., 4-class) classification problem of the DFUC2021 dataset. Here, we employ histogram equalization and a CNN-based approach to produce color and sharpness enhanced DFU images. We propose integrating these color and sharpness enhanced DFU images with the original DFU images to overcome image quality issues e.g., blurriness and inconsistent lighting. Furthermore, we adopt an optimization technique, namely adaptive sharpness-aware minimization (ASAM), to improve model generalization performance. We fine-tune the parameters of this optimization technique to use in our network. In addition, we present a novel approach to interpret all four class probabilities from multi-label classifier outputs using Venn diagram representation and its associated

likelihood equations. Our proposed method achieves the highest classification performance compared to all other methods using the DFUC2021 dataset.

2 Proposed Method

In this section, we briefly describe our main methodological aspects of solving the DFU image classification problem that include preparation of dataset, color and sharpness enhancement, improving generalization performance, multi-label classification and network architecture.

2.1 Dataset

The DFUC2021 dataset is available for research purposes following application procedures listed in the official website of DFUC2021. The dataset focuses on assessing and analyzing infection and ischaemia in images of DFUs Yap et al. [2021b]. These images were taken from the patients during clinical visits at Lancashire Teaching Hospitals. Three cameras were used to take the foot images: a Kodak DX4530, a Nikon D3300, and a Nikon COOLPIX P100. The images were taken in room lights from a distance of 30–40 cm with a parallel orientation to the plane of an ulcer. The DFU areas are clipped from the original photos, and natural data augmentation is carried out by maintaining the case id. This pipeline yielded 15,683 DFU images. Following that, these images are divided into three different subgroups (with exclusive image id), i.e., 5,955 (37.97%) labelled training images, 3,994 (25.47%) unlabelled training images, and 5,734 (36.56%) test images. The labelled images are categorized into four classes: infection, ischaemia, both infection and ischaemia (both), or none of infection and ischaemia (control). The distribution of the labelled training images among the classes are as follows: 2,555 (42.91%) infection images, 227 (3.81%) ischaemia images, 621 (10.43%) both images, and 2,552 (42.85%) control images.

2.2 Data Augmentation

Despite being the largest dataset of its kind, DFUC2021 has extremely uneven distribution of images and it is still insufficient to train deep network. Therefore, it is necessary to apply data augmentation to generalize the model. We added augmentations using Albumentations library[2]. We used the following augmentations: horizontal flip, vertical flip, random contrast, random brightness, RGB shifting, scaling, and rotation. We performed all augmentation operations on the given input image size of 224×224 pixels.

2.3 Histogram Equalization and Sharpness Enhancement

The presence of poor reperfusion to the foot or appearance of black gangrenous toes may indicate the presence of ischaemia, and increased redness in and around the ulcer, as well as colored purulent, could be signs of infection Goyal et al. [2020b]. According to these observations, color and texture information of the wounds are critical features that can aid in DFU classification. However, a large number of DFU images lack accurate color and texture information due to blurriness and inconsistent lighting. Motivated by these observations, we perform histogram equalization and sharpness enhancement on the DFUC2021 dataset.

Since only gray scale images have a well-defined histogram, applying histogram equalization to color images is a difficult task. It involves applying histogram equalization individually to each channel of an RGB image. The effect of histogram equalization on the DFUC2021 dataset can be visualized in the second row of Fig. 1. We used the trained model in Guo et al. [2019] to generate the sharpness enhanced DFU images. It is originally a dehazing network that uses a DenseNet-based feature encoder with three different DensetNet-based decoders producing estimates of the image's R, G, and B color channels. Sharpness enhanced DFU images can be visualized in the third row of Fig. 1.

2.4 Adaptive Sharpness-Aware Minimization

The term "generalization" refers to the ability of a trained deep neural network to classify unseen data Nasir et al. [2021]. Deep learning utilizes gradient-based optimizers such as Stochastic Gradient Descent (SGD) or Adaptive Moment Estimation (ADAM) to find a local minimum for a loss surface of training data, which indirectly minimizes generalization loss.

Galdran et al. Galdran et al. [2022] showed the impact of using sharpness-aware minimization (SAM) Foret et al. [2020] with SGD optimizer. In this paper, we investigated the impact of using adaptive sharpness-aware minimization

[2]https://github.com/albumentations-team/albumentations

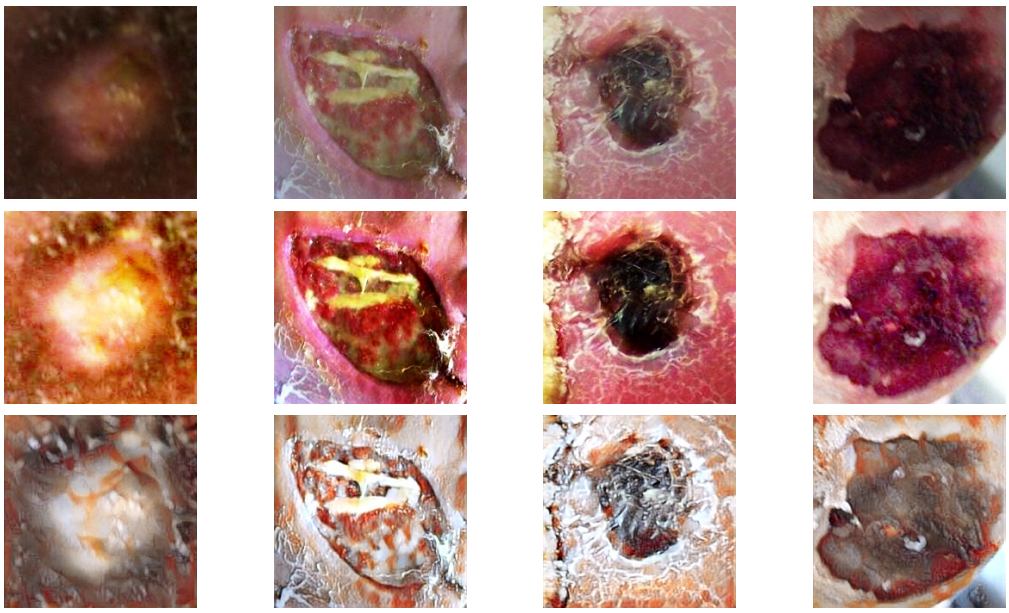

(a) Control (b) Infection (c) Ischaemia (d) Both

Figure 1: Visualization of original images (first row), histogram equalized images (second row), and sharpness enhanced images (third row).

(ASAM) with Adam optimizer. Motivated by the relationship between generalization metrics and loss minimization, ASAM adaptively adjusts maximization regions in response to parameter re-scaling Kwon et al. [2021]. Moreover, it minimizes the corresponding generalization bound using adaptive sharpness to generalize on unseen data, hence eliminating the scale-dependency issue that SAM suffers from Kwon et al. [2021]. The parameters of the ASAM technique have been fine-tuned to ensure that it applies to our network.

2.5 Multi Label Classification

A significant challenge of the dataset was to identify both class images correctly. As both class images have combined infection and ischaemia class features, it was difficult for a model to correctly distinguish between both class, infection class, and ischaemia class. Since both class wounds are defined as the simultaneous presence of infection and ischaemia a, whereas none class wounds are defined as the absence of infection and ischaemia, we propose to use multi-label classification approach. In multi-label classification, an input is allowed to have multiple classes which simplifies the four class classification problem to a two class classification problem. To interpret all the four class probabilities from

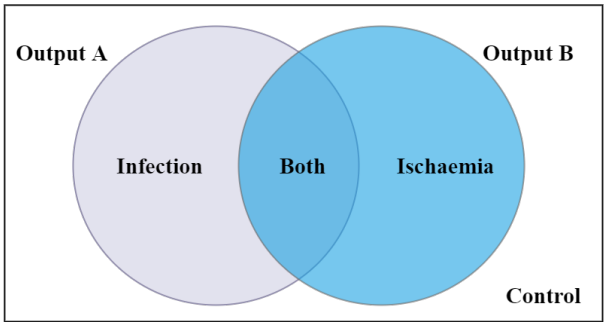

Figure 2: Visualization of the dependency between the 4 classes using Venn Diagram.

these two classes, we propose a novel Venn Diagram representation block in classifier, shown in Fig. 2. Here, Output A and Output B represent outputs from the two sigmoid layers in the proposed network architecture, shown in Fig. 4. The

four class probabilities can be obtained from the following equations,

$$\mathcal{P}(both) = \mathcal{P}(output\ A\ \cap\ output\ B) \tag{1}$$

$$\mathcal{P}(control) = \mathcal{P}(\overline{output\ A})\ \cap\ \mathcal{P}(\overline{output\ B}) \tag{2}$$

$$\mathcal{P}(infection) = \mathcal{P}(output\ A\ \cap\ \overline{output\ B}) \tag{3}$$

$$\mathcal{P}(ischaemia) = \mathcal{P}(\overline{output\ A}\ \cap\ output\ B) \tag{4}$$

2.6 Squeeze-and-Excitation Block

The Squeeze-and-Excitation Block (SE Block) is a building block of Squeeze-and-Excitation Networks (SENets) Hu et al. [2018]. Convolutional neural networks extract spatial data from each input channel and combine the information across all possible output channels using convolutional filters Hoang and Jo [2021]. While constructing the output feature maps, the network weights each channel equally. SE blocks are used to change this trend by incorporating a content-aware method for adaptively weighting each channel. An SE block, see Fig. 3, takes a convolutional block as an input. Each channel in the convolutional block is reduced to a single numeric value by using global average pooling (GAP). Non-linearity is introduced using a dense layer followed by a ReLU activation, which reduces output channel complexity by a factor (r). Another fully connected (FC) layer followed by a sigmoid gives each channel a smooth gating function. Next, each feature map is given a weight based on the side network's output, called "excitation". These steps incur a negligible additional computational cost and can be applied to any model.

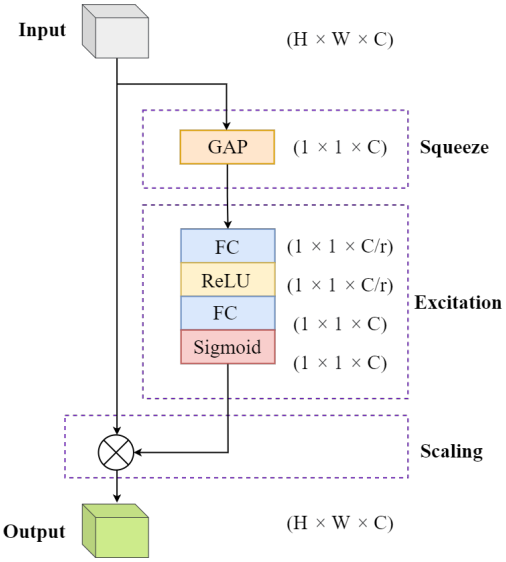

Figure 3: Squeeze-and-Excitation Block.

2.7 Implementation

2.7.1 Training

We conduct histogram equalization and sharpness enhancement on original images individually during the first stage of the training phase. Then, we concatenate these images such that the original image and its enhanced version remains in the same batch. This concatenation allows the model to learn features from the original and enhanced image versions concurrently, improving generalization performance. Same set of augmentations (horizontal flip, vertical flip, random contrast, random brightness, RGB shifting, scaling, and rotation) are applied on these images. To employ multi-label classification, we labeled our dataset images as infection - 10, ischaemia - 01, both - 11, control - 00 compared to infection - 0, ischaemia - 1, both - 2, control - 3 in multi-class classification. As in multi-label classification an input is allowed to have multiple classes; occurrence of both or control class can be determined from individual infection and ischaemia probabilities which simplifies the challenge of four-class classification to a two-class classification problem.

We conducted our experiments using PyTorch Paszke et al. [2019] as the deep learning framework. In the benchmark study Yap et al. [2021b], EfficientNet-B0 outperformed other pre-trained convolutional networks in terms of classification performance. Therefore, we conducted our experiments using EfficientNet Tan and Le [2019] architectures as

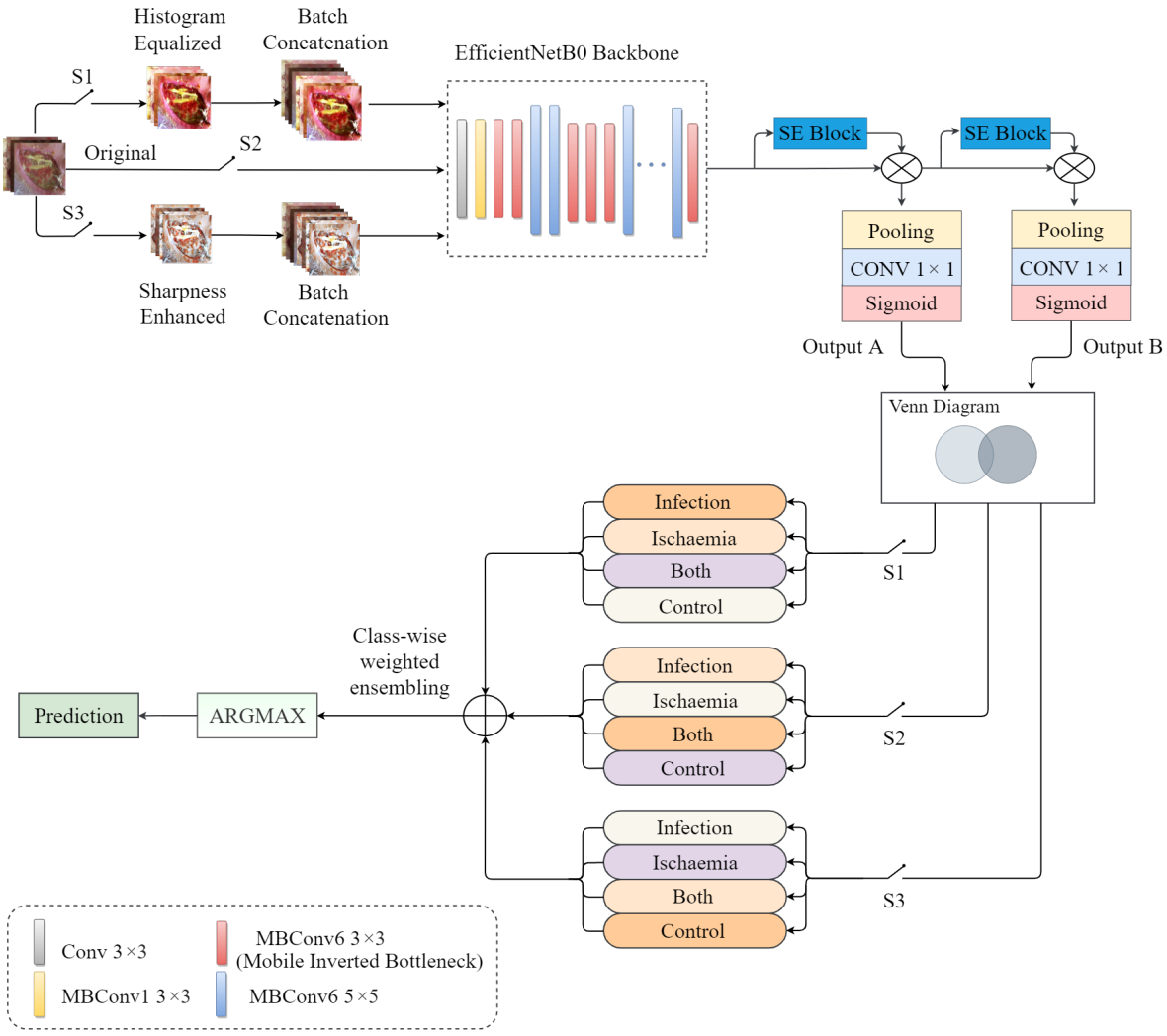

Figure 4: Proposed network architecture for multi-label diabetic foot ulcer classification.

backbone. We have used four versions of EfficientNet architecture, namely EfficientNetB0, EfficientNetB1, EfficientNetB2 and EfficientNetB3. All the models were pre-trained on ImageNet datasets. We experimented with the settings of various hyperparameters such as learning rate, batch size, number of epochs, oversampling techniques, optimizer, and drop out rate. The best performing hyperparameters for various EfficientNet architectures are listed in Table 1.

EfficientNet backbone processes these input DFU images and generates a feature map fed into a classifier block. The classifier block has a SE block as an initial layer that performs dynamic channel-wise feature re-calibration. Then, we aggregate this information by using both average-pooling and max-pooling operations. The aggregated feature vector is passed through a fully connected (FC) layer built as a 1×1 convolutional layer, which returns a class activation score. We further bound it with the sigmoid function, and the output is interpreted as the wound class probability. Output feature map of the initial SE block is further fed into a second SE block, which goes through the same pooling and FC layers configuration as the first and produces the other wound class probability.

In this work, we perform multi-label classification of input DFU images. Multi-label classification approach simplifies this 4-class classification problem into a 2-class classification problem. Therefore, we use Binary Cross-Entropy (BCE) as the loss function that compares each predicted probability to the actual output which can be either 0 or 1. After applying sigmoid activation on the predicted output of the network, the BCE loss can be calculated using Equation 5.

$$\text{BCE Loss} = -\frac{1}{\text{N}}\sum_{i=1}^{\text{N}} y_i \cdot \log \hat{y}_i + (1 - y_i) \cdot \log (1 - \hat{y}_i) \tag{5}$$

Table 1: Hyperparameters used to train the EfficientNet models.

Parameters	**B0**	**B1**	**B2**	**B3**
Learning Rate	0.0001	0.0001	0.0001	0.0001
Batch Size	100	100	100	70
Oversampling	×	✓	×	×
Scheduler	×	×	✓	✓
No. of Epochs	70	100	70	70
Optimizer	Adam	Adam	Adam	Adam
Drop Out	0.3	0.3	0.3	0.3

where $\hat{y}_i$ is model prediction of the i-th image, y_i is the corresponding ground truth, and N is the number of images in a batch.

An appropriate learning rate and learning rate scheduler are chosen depending on the value of the loss function. Learning rate of 0.0001 and step learning rate scheduler with gamma 0.1 and step-size 10 are used. It decays the learning rate of each parameter group by 0.1 in every 10 epochs.

2.7.2 Testing

Test dataset images of DFUC2021 are fed into EfficientNet feature extractors, and the extracted feature map is input into the classifier block. To calculate the four-class probabilities from the outputs (Output A and Output B) of the classifier block, we propose a novel approach of using a Venn diagram representation, shown in Fig. 2, and its associated likelihood equations (1-4), e.g., a DFU input image with classifier outputs of 0.7 as output A and 0.45 as output B will be interpreted as $\mathcal{P}$(control) = 0.165, $\mathcal{P}$(both) = 0.315, $\mathcal{P}$(infection) = 0.385, and $\mathcal{P}$(ischaemia) = 0.135. Using maximum likelihood, the DFU input image will be classified as an infection. Similarly, a DFU input image with classifier outputs of 0.8 and 0.6 as output A and output B, respectively, the interpreted probability values will be as follows: $\mathcal{P}$(control) = 0.08, $\mathcal{P}$(both) = 0.48, $\mathcal{P}$(infection) = 0.32, and $\mathcal{P}$(ischaemia) = 0.12. Therefore, the DFU input image will be classified as an occurrence of both of the conditions.

Probability values are determined in the same manner for EfficientNetB0, EfficientNetB1, EfficientNetB2, EfficientNetB3 and then averaged for each input image. The final prediction results from multiple dataset versions (original, histogram equalized, and sharpness enhanced) are classwise weighted and ensembled. Weights of 0.15, 0.25, 0.3, and 0.3 are chosen iteratively for control, infection, ischaemia, and both classes, respectively.

2.7.3 Performance Metrics

We evaluate the performance of our proposed approach using precision, recall, F1-score, and area under the Receiver Operating Characteristics Curve (AUC). As the class distribution of the DFUC2021 dataset is imbalanced, the performance metrics are reported in macro-average scale. In imbalanced dataset situations, macro-average scoring is utilized because it puts equal emphasis on minority classes Yap et al. [2021b]. As the DFUC2021 leaderboard is based on the macro-average F1-score, this metric is chosen as the primary evaluation metric. Macro-average F1-score is defined as the arithmetic mean of all the per class F1-Scores, i.e.,

$$\text{F1}_i = \frac{2 * TP_i}{2 * TP_i + FP_i + FN_i} \tag{6}$$

$$\text{Macro–average F1–score} = \frac{1}{\text{N}} \sum_{i=1}^{\text{N}} \text{F1}_i \tag{7}$$

where, N represents the total number of classes. TP_i, FP_i, and FN_i are True Positives, False Positives, and False Negatives, respectively, for each class *i*.

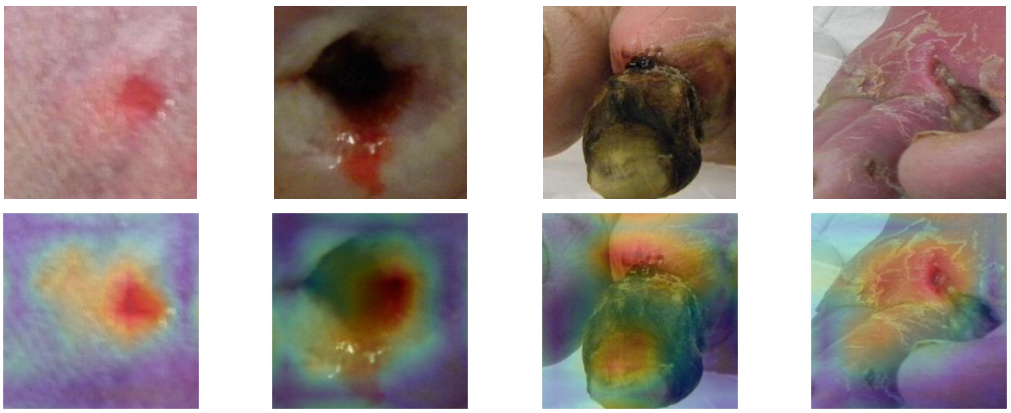

(a) (b) (c) (d)

Figure 5: Illustration of original image patches (first row) and its corresponding GRAD-CAM output (second row) of our proposed network. From left to right: (a) Control, (b) Infection, (c) Ischaemia, and (d) Both.

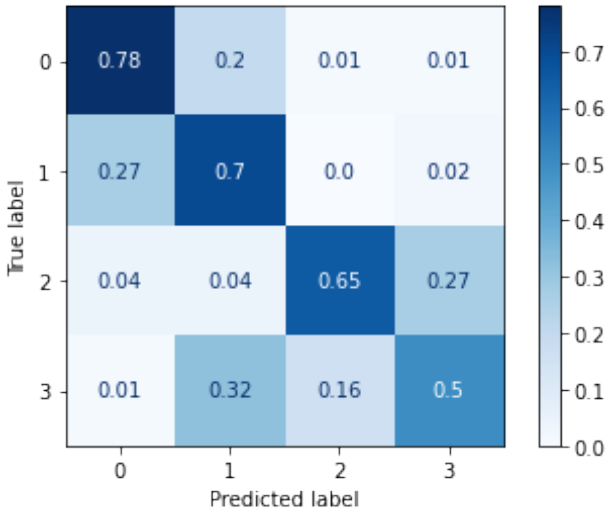

Figure 6: Confusion matrix of the proposed approach. Labels correspond to, 0- None, 1- Infection, 2- Ischaemia, 3- Both.

Table 2: Results of class-wise weighted ensembling of models using original, histogram equalized, and sharpness enhanced dataset.

Classes	**Precision**	**Recall**	**F1-score**	**AUC**
Control	0.7382	0.7819	0.7594	0.8494
Infection	0.7272	0.7023	0.7145	0.8203
Ischaemia	0.5573	0.6489	0.5996	0.9688
Both	0.6383	0.5042	0.5634	0.9391
Macro-Average	0.6652	0.6593	0.6592	0.8945
Accuracy	0.7187	-	-	-

Table 3: Quality measurements of the original DFU image and its enhanced versions. Lower score indicates better image quality.

Condition	Image	BRISQUE	NIQE	PIQE
Blurred	Original	54.93	4.47	92.59
	Histogram Equalized	18.75	4.02	44.77
	Sharpness Enhanced	36.58	3.30	36.91
Inconsistent Lighting	Original	44.06	5.21	37.20
	Histogram Equalized	33.67	4.82	15.90
	Sharpness Enhanced	23.09	3.56	25.08

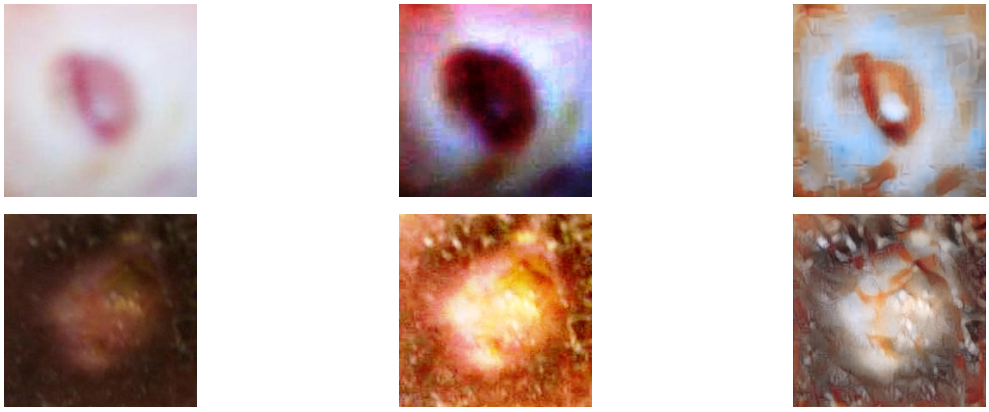

Figure 7: Visualization of a blurred DFU image, its histogram equalized version, and its sharpness enhanced version, respectively (first row) and a DFU image with inconsistent lighting, its histogram equalized version, and its sharpness enhanced version, respectively (second row).

3 Results and Discussion

The performance of the proposed model for addressing the four-class classification problem of finding whether a DFU image falls in the category of infection, ischaemia, both of these conditions, or none of these conditions (control) is reported in this section. Our proposed approach involves training the model with the original DFUC2021 training dataset and its histogram-equalized and sharpness-enhanced versions. Class-wise weighted ensembling is used to combine the advantages of these different trained models to maximize each class's performance. To show that our model extracts discriminative features from the right region of a DFU wound, we present the GRAD-CAM output of DFU images for each class in Fig. 5. These images were not included in training to demonstrate the model's performance on unseen data. The red and green colors in each image represent the discriminative image regions that the model focuses on. It appears that employing the SE block in the classifier enables more precise localization of the DFU wound region. The confusion matrix of our proposed approach is depicted in Fig 6. These results demonstrate that our proposed approach has good potential distinguishing infection class from ischaemia class as there is no confusion between them.

It is to be noted that the ground truth of the DFUC2021 testing dataset has not yet been made public. To evaluate the model prediction on the test dataset, one must generate a CSV file with the class probability for each image in separate columns and upload it to the official challenge website.[3]

3.1 Experimental Results

Table 2 reports the performance of the class-wise weighted ensembling of the different trained models evaluated with the DFUC2021 test dataset. The proposed approach achieves macro-average scores of 0.6592 for precision, 0.6593 for recall, and 0.6592 for F1-score, respectively.

A performance comparison between the baseline and top-3 winning papers from DFUC2021 is shown in Table 4. Our proposed approach outperforms all other approaches in all classification performance metrics, particularly in infection

[3]https://dfu-2021.grand-challenge.org/evaluation/submissions/

and ischaemia classes. Moreover, in Cassidy et al. [2022], Cassidy et al. ensembled these top-3 performing models from the DFUC2021 and reported macro-average scores of 0.6352 for precision, 0.6422 for recall, and 0.6307 for F1-score. Our model still outperforms the ensembling results with a good margin in terms of overall performance.

Table 4: Comparison of different approaches for DFU classification using DFUC2021 test dataset.

	Per Class F1-Score				Macro-average			
Methods	Control	Infection	Ischaemia	Both	Precision	Recall	F1-score	AUC
Baseline Yap et al. [2021b]	0.73	0.56	0.44	0.47	0.57	0.62	0.55	0.86
Ahmed et al Ahmed and Naveed [2022]	0.7157	0.6714	0.4574	0.5390	0.5984	0.5979	0.5959	0.8644
L. Bloch et al. Bloch et al. [2022]	0.7453	0.5917	0.5579	0.5358	0.6206	0.6246	0.6077	0.8616
A. Galdran et al. Galdran et al. [2022]	0.7574	0.6387	0.5282	0.5619	0.6139	0.6521	0.6215	0.8855
Proposed Method	**0.7594**	**0.7145**	**0.5996**	**0.5634**	**0.6652**	**0.6593**	**0.6592**	**0.8945**

Table 5: Ablation experiments using different combinations of original and enhanced datasets.

Dataset	ASAM	Precision	Recall	F1 Score	AUC	Accuracy
Original	×	0.6283	0.6123	0.6124	0.8707	0.6676
Original	✓	0.6443	0.6346	0.6283	0.8830	0.6730
Original + Histogram Equalized	✓	0.6551	0.6580	0.6522	0.8899	0.7051
Original + Histogram Equalized + Sharpness Enhanced (Proposed)	✓	**0.6652**	**0.6593**	**0.6592**	**0.8945**	**0.7187**

3.2 Ablation Studies

To demonstrate the impact of the components, e.g., ASAM, image enhancement strategies (i.e., histogram equalization and sharpness enhancement) adopted in our algorithm, we perform several ablation experiments.

For measuring the effect of image enhancement techniques (i.e., histogram equalization and sharpness enhancement) on DFU images, we consider three standard image quality metrics, namely BRISQUE, NIQE, and PIQE. Here, BRISQUE evaluates spatial quality Mittal et al. [2012], NIQE evaluates naturalness of a image Mittal et al. [2013], and PIQE evaluates perceptual image quality N et al. [2015]. These metrics are preferred for image quality evaluation because they require no reference image. It is to be noted that, when these three measures have low values, it indicates that the image quality is better. In Fig. 7, we compare DFU images with blurring and inconsistent lighting with their enhanced versions. The image quality metrics score for these images are reported in Table 3. It is clear from the results that histogram equalized images and sharpness enhanced images are superior in terms of image quality. Therefore, these image enhancement techniques help in overcoming the blurriness and lighting inconsistency of DFU images.

In Table 5, we report the results of other ablation experiments. Without ASAM, classification performance decreases across the board. After including ASAM, classification performance improves by 2.59% in terms of macro-average F1-score. Therefore, it is clear that employing adaptive sharpness-aware optimization during training has a beneficial effect. Next, the model trained with histogram equalized DFU images is class-wise weighted and ensembled with the existing model. This inclusion significantly improves all performance metrics, with a macro-average F1-score of 0.6522, up from 0.6283 previously. Then, the model trained with sharpness enhanced DFU images is ensembled similarly to existing datasets. Although this addition has minimal impact on overall classification performance, the usefulness of this strategy is better understandable at class level performance, e.g., infection class F1-score has an improved to 0.7145, up from 0.6834 previously (about 4.55% increment). The experiments show that combining all the datasets has the highest impact on the macro-average performance. Therefore, it justifies the idea of generating color and sharpness enhanced datasets and their uses in combination with the original DFUC2021 dataset.

4 Conclusion

In this paper, a multi-label CNN-based approach utilizing different image enhancement strategies for DFU classification has been proposed. We have demonstrated that combining color and sharpness enhanced images along with original images overcomes the blurriness and inconsistent lighting effect of DFU images, and this inclusion significantly improves DFU classification performance. As the dataset is highly imbalanced and somewhat small, we have employed

an optimization technique, namely adaptive sharpness-aware minimization, to improve the models' generalization performance. We have also incorporated a squeeze-and-excitation block in the classifier to improve the network's content-awareness ability. Furthermore, we have introduced a novel approach of using Venn diagram representation and its associated event likelihood equations to calculate all four class probabilities from classifier outputs. In this paper, we have used the largest international DFU pathology dataset, and our work has presented the best-performing solution to this dataset. We believe our proposed solution contribute to the development of automatic classification of DFU, which is a crucial step for early identification and prevention of limb amputation and possibly death.

5 Conflict of interest

There is no conflict of interest in this work.

References

Hong Sun, Pouya Saeedi, Suvi Karuranga, Moritz Pinkepank, Katherine Ogurtsova, Bruce B. Duncan, et al. IDF diabetes atlas: Global, regional and country-level diabetes prevalence estimates for 2021 and projections for 2045. *Diabetes Res. Clin. Pract.*, 183:109119, January 2022. doi:10.1016/j.diabres.2021.109119. URL `https://doi.org/10.1016/j.diabres.2021.109119`.

David G. Armstrong, Andrew J.M. Boulton, and Sicco A. Bus. Diabetic foot ulcers and their recurrence. *N. Engl. J. Med.*, 376(24):2367–2375, June 2017. doi:10.1056/nejmra1615439. URL `https://doi.org/10.1056/nejmra1615439`.

Ejiofor Ugwu, Olufunmilayo Adeleye, Ibrahim Gezawa, Innocent Okpe, Marcelina Enamino, and Ignatius Ezeani. Predictors of lower extremity amputation in patients with diabetic foot ulcer: findings from MEDFUN, a multi-center observational study. *J. Foot Ankle Res.*, 12(1), June 2019. doi:10.1186/s13047-019-0345-y. URL `https://doi.org/10.1186/s13047-019-0345-y`.

Bill Cassidy, Connah Kendrick, Neil D. Reeves, Joseph M. Pappachan, Claire O'Shea, David G. Armstrong, and Moi Hoon Yap. Diabetic foot ulcer grand challenge 2021: Evaluation and summary. In Moi Hoon Yap, Bill Cassidy, and Connah Kendrick, editors, *Diabetic Foot Ulcers Grand Challenge*, volume 13183, pages 90–105, Cham, 2022. Springer International Publishing. ISBN 978-3-030-94907-5. doi:10.1007/978-3-030-94907-5_7.

Jaap J. van Netten, Damien Clark, Peter A. Lazzarini, Monika Janda, and Lloyd F. Reed. The validity and reliability of remote diabetic foot ulcer assessment using mobile phone images. *Sci. Rep.*, 7(1), August 2017. doi:10.1038/s41598-017-09828-4. URL `https://doi.org/10.1038/s41598-017-09828-4`.

Manu Goyal, Neil D. Reeves, Adrian K. Davison, Satyan Rajbhandari, Jennifer Spragg, and Moi Hoon Yap. DFUNet: Convolutional neural networks for diabetic foot ulcer classification. *IEEE Trans. Emerg. Top. Comput. Intell.*, 4 (5):728–739, October 2020a. doi:10.1109/tetci.2018.2866254. URL `https://doi.org/10.1109/tetci.2018.2866254`.

Manu Goyal, Neil D. Reeves, Satyan Rajbhandari, and Moi Hoon Yap. Robust methods for real-time diabetic foot ulcer detection and localization on mobile devices. *IEEE J. Biomed. Health Inform.*, 23(4):1730–1741, 2019. doi:10.1109/JBHI.2018.2868656.

Manu Goyal, Neil D. Reeves, Satyan Rajbhandari, Naseer Ahmad, Chuan Wang, and Moi Hoon Yap. Recognition of ischaemia and infection in diabetic foot ulcers: Dataset and techniques. *Comput. Biol. Med*, 117:103616, February 2020b. doi:10.1016/j.compbiomed.2020.103616. URL `https://doi.org/10.1016/j.compbiomed.2020.103616`.

B Cassidy, ND Reeves, P Joseph, D Gillespie, C O'Shea, S Rajbhandari, AG Maiya, E Frank, A Boulton, D Armstrong, et al. The DFUC 2020 dataset: Analysis towards diabetic foot ulcer detection. *Eur. Endocrinol.*, 1(1):5, 2021. doi:10.17925/ee.2021.17.1.5. URL `https://doi.org/10.17925/ee.2021.17.1.5`.

Moi Hoon Yap, Ryo Hachiuma, Azadeh Alavi, Raphael Brüngel, Bill Cassidy, Manu Goyal, et al. Deep learning in diabetic foot ulcers detection: A comprehensive evaluation. *Comput. Biol. Med.*, 135:104596, August 2021a. doi:10.1016/j.compbiomed.2021.104596. URL `https://doi.org/10.1016/j.compbiomed.2021.104596`.

Moi Hoon Yap, Bill Cassidy, Joseph M. Pappachan, Claire O'Shea, David Gillespie, and Neil D. Reeves. Analysis towards classification of infection and ischaemia of diabetic foot ulcers. In *2021 IEEE EMBS Int. Conf. Biomed. Health Inform.*, pages 1–4, 2021b. doi:10.1109/BHI50953.2021.9508563.

Adrian Galdran, Gustavo Carneiro, and Miguel A. González Ballester. Convolutional nets versus vision transformers for diabetic foot ulcer classification. In Moi Hoon Yap, Bill Cassidy, and Connah Kendrick, editors, *Diabetic Foot*

Ulcers Grand Challenge, pages 21–29, Cham, 2022. Springer International Publishing. ISBN 978-3-030-94907-5. doi:10.1007/978-3-030-94907-5_2.

Pierre Foret, Ariel Kleiner, Hossein Mobahi, and Behnam Neyshabur. Sharpness-aware minimization for efficiently improving generalization, 2020.

Jungmin Kwon, Jeongseop Kim, Hyunseo Park, and In Kwon Choi. ASAM: Adaptive sharpness-aware minimization for scale-invariant learning of deep neural networks. In *38th Int. Conf. Mach. Learn.*, volume 139, pages 5905–5914. PMLR, 18–24 Jul 2021.

Louise Bloch, Raphael Brüngel, and Christoph M. Friedrich. Boosting efficientnets ensemble performance via pseudo-labels and synthetic images by pix2pixhd for infection and ischaemia classification in diabetic foot ulcers. In Moi Hoon Yap, Bill Cassidy, and Connah Kendrick, editors, *Diabetic Foot Ulcers Grand Challenge*, pages 30–49, Cham, 2022. Springer International Publishing. ISBN 978-3-030-94907-5. doi:10.1007/978-3-030-94907-5_3.

Salman Ahmed and Hammad Naveed. Bias adjustable activation network for imbalanced data—diabetic foot ulcer challenge 2021. In Moi Hoon Yap, Bill Cassidy, and Connah Kendrick, editors, *Diabetic Foot Ulcers Grand Challenge*, pages 50–61, Cham, 2022. Springer International Publishing. ISBN 978-3-030-94907-5. doi:10.1007/978-3-030-94907-5_4.

Tiantong Guo, Venkateswararao Cherukuri, and Vishal Monga. Dense '123' color enhancement dehazing network. In *Proc. IEEE Comput. Soc. Conf. Comput. Vis. Pattern Recognit.*, pages 2131–2139, 2019. doi:10.1109/CVPRW.2019.00266.

Jamal Abdul Nasir, Osama Subhani Khan, and Iraklis Varlamis. Fake news detection: A hybrid CNN-RNN based deep learning approach. *International Journal of Information Management Data Insights*, 1(1):100007, April 2021. doi:10.1016/j.jjimei.2020.100007. URL `https://doi.org/10.1016/j.jjimei.2020.100007`.

Jie Hu, Li Shen, and Gang Sun. Squeeze-and-excitation networks. In *2018 Proc. IEEE Comput. Soc. Conf. Comput. Vis. Pattern Recognit.*, pages 7132–7141, 2018. doi:10.1109/CVPR.2018.00745.

Van-Thanh Hoang and Kang-Hyun Jo. Practical analysis on architecture of efficientnet. In *14th Int. Conf. Hum. Syst. Interact. HSI*, pages 1–4. IEEE, 2021. doi:10.1109/HSI52170.2021.9538782.

Adam Paszke, Sam Gross, Francisco Massa, Adam Lerer, James Bradbury, Gregory Chanan, Trevor Killeen, Zeming Lin, Natalia Gimelshein, Luca Antiga, et al. Pytorch: An imperative style, high-performance deep learning library. *Adv. Neural Inf. Process. Syst.*, 32, 2019.

Mingxing Tan and Quoc Le. EfficientNet: Rethinking model scaling for convolutional neural networks. In *36th Int. Conf. Mach. Learn.*, volume 97, pages 6105–6114. PMLR, 2019.

Anish Mittal, Anush Krishna Moorthy, and Alan Conrad Bovik. No-reference image quality assessment in the spatial domain. *IEEE Trans. Image Process.*, 21(12):4695–4708, 2012. doi:10.1109/TIP.2012.2214050.

Anish Mittal, Rajiv Soundararajan, and Alan C. Bovik. Making a "completely blind" image quality analyzer. *IEEE Signal Process. Lett.*, 20(3):209–212, 2013. doi:10.1109/LSP.2012.2227726.

Venkatanath N, Praneeth D, Maruthi Chandrasekhar Bh, Sumohana S. Channappayya, and Swarup S. Medasani. Blind image quality evaluation using perception based features. In *Proc. 25th Nat. Conf. Commun.*, pages 1–6, 2015. doi:10.1109/NCC.2015.7084843.